CHAPTER

7

Kinematics of Pure Shear Ductile Deformation Within Rigid Walls: New Analyses

Soumyajit Mukherjee

Department of Earth Sciences, Indian Institute of Technology Bombay, Powai, Mumbai, India

OUTLINE

1 INTRODUCTION

Pure shear deformation is one of the end members of the ductile shearing phenomenon in structural geology and tectonics that work at widely different tectonic domains and from a depth usually exceeding 8 or 15 km in the ductile regime (Passchier and Trouw, 2005). In such a deformation, the two long rigid boundaries/margins of a ductile shear zone, considered parallel in most of the cases, move toward (or away from) each other perpendicular to their lengths. Secondary synthetic and antithetic shears in ductile shear zones in meso- and microscales probably indicate a pure shear component (Mukherjee, 2013). Natural ductile shear zones have been reported to usually have one more deformation component, viz., simple shear/Couette flow (=pure shear of Gere and Goodno, 2012; see Xypolias, 2010 and Bose et al., 2018 as examples). Besides, pure shear kinematics is one of the ways to explain rifting (Fig. 1A) and nappe movement/gravitational spreading (Fig. 1B) (e.g., Fossen, 2016).

Analyzing ductile shear in terms of pure and simple shear components have been in practice for more than 100 years in geoscience (Howarth, 2017). There has also been significant discussion regarding pure shear (and simple shear) in material science (Segal, 2002). In particular, velocity at any point in a shear zone, pure, simple, or general, has been presented in Jaeger (1969). Simple and pure shear, if operating together, is called subsimple or general shear. Understanding kinematics of shear zones is of great importance in deciphering plate tectonics, rheology, and seismicity (e.g., Regenauer-Lieb and Yuen, 2003; Hobbs and Ord, 2014; Mulchrone and Mukherjee, 2016; Fossen and Cavalcante, 2017).

Pure shear mechanism can work on some flowing lavas as well (Manga, 2005). Such shear kinematics has been worked out from different perspectives in mechanics/rheology works (e.g., Segal, 2002; "Stephan's squeezing flow" in Papanastasiou et al., 2000; Malkin and Isayev, 2006). The deformation involves parabolic flow path of fluid particles (Schlichting, 1960). However, how it would deform straight marker layers was not analyzed properly, even though pure shear is referred frequently in structural geological texts (e.g., Dennis, 1987; Reitan, 1987; Twiss and Moores, 2007; Fossen, 2016). The other detail of pure shear of two media has been available. For example, Treagus and Lan (2000) studied the mode of deformation of square objects within another medium under pure shear.

Developments in Structural Geology and Tectonics, Volume 5
https://doi.org/10.1016/B978-0-12-814048-2.00007-7

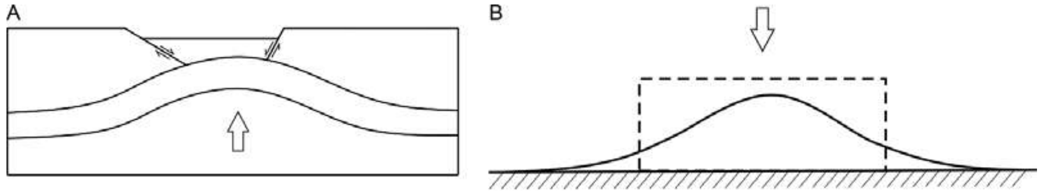

FIG. 1 (A) Pure shear-induced rifting. The uprising magma body exerts pure shear on the overlying rock body. (B) Gravitational spreading by its own exerts pure shear on the spreading mass.

This work elaborates kinematics of pure shear presuming ductile rocks to be a single incompressible Newtonian viscous fluid. Such a consideration has yielded other first order understanding of ductile shear zones (e.g., Ramsay and Lisle, 2000; Mukherjee, 2012). Pure shear-dominated ductile shear zones do exist in nature (e.g., Bailey et al., 2007) where this analysis could approximately apply. However, a natural shear zone with only pure shear and zero simple shear has not yet been reported to the knowledge of the author.

A. ***Instruction to the Instructor****:* The prerequisite knowledge for students here would be elementary calculus. We are going to do an area-balancing exercise, typically what is done for cross-section balancing (e.g., Lopez-Mir, 2018). Our aim is to find the equation of the velocity profile for pure shear. Step-wise, present the following materials to students. Give them sufficient time to solve equations independently.

2 PURE SHEAR KINEMATICS

2.1 One Boundary Stationary and the Other Moves

Consider a rectangle $ABCD$ with a rigid base BC. Side AD is compressed with a constant velocity V. After instant "t," AD comes to $A'D'$. The incompressible Newtonian viscous fluid expels at the two free sides as parabolic profiles P_1 and P_2. With the chosen coordinates as in Fig. 2A, $AA' = V{\cdot}t$, therefore area $AA'DD' = L{\cdot}(V{\cdot}t)$. P_1 is represented by:

$$x = Ay^2 + By + C \tag{1}$$

$$\text{As this parabola passes through the origin } (0, 0), \text{ therefore } C = 0 \tag{2}$$

$$\text{Or, } x = Ay^2 + By \tag{3}$$

B. ***Instruction to the Instructor****:* Ask students what will be the problem if the origin is chosen differently. Also, one needs to inform the students that the profile need not be parabolic for other rheology of the fluid.

The origin is chosen in this way to simplify Eq. (1). This does not modify the physical process of deformation. Rather the representation is simplified. And as it passes through point $A'[0, (y_0 - Vt)]$, putting $x = 0$ and $y = (y_0 - Vt)$ in Eq. (3) and simplifying:

$$B = -A(y_0 - Vt) \tag{4}$$

Now, the area bound by the line AB (or the Y-axis) and the parabola P_1:

$$A_1 = \int_0^{(y_0 - Vt)} x\mathrm{d}x \tag{5}$$

Putting the expression for "x" from Eq. (3) into Eq. (5) and integrating:

$$A_1 = (y_0 - Vt)^2[0.33{*}A(y_0 - Vt) + 0.5{*}B] \tag{6}$$

Considering that the area lost by compression [i.e., area $AA'DD' = L{\cdot}(V{\cdot}t)$] would be equally distributed at the two parabolic sides, that is,

$$A_1 = 0.5LVt \tag{7}$$

Equating A_1 from Eqs. (6) and (7), and using Eq. (4):

$$A = -3VtL(y_0 - Vt)^{-3} \tag{8}$$

$$B = 3{*}VtL(y_0 - Vt)^{-2} \tag{9}$$

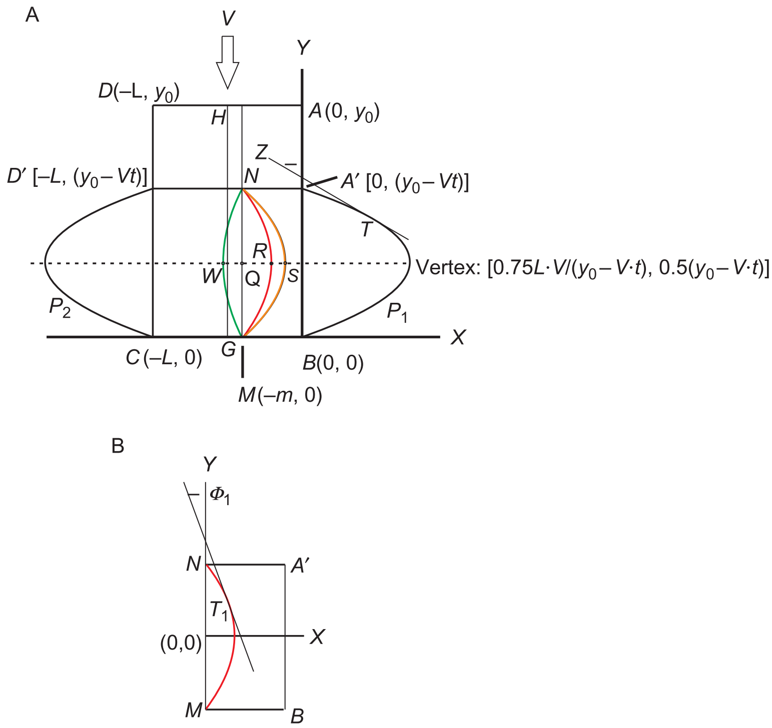

FIG. 2 (A) Pure shear on rectangle *ABCD* on side *AD* with a velocity "*V*." Side *BC* places rigidly on the *X*-axis. Line *AD* moves to *A′D′* after time "*t*." Had *A′BMN* been the only rectangle present, line *NG* would have been deformed as the green parabolic profile. Had *ND′CM* been the only rectangle present, line *NG* would have been deformed as the orange parabola. When both the rectangles are present, that is, when we consider the rectangle *A′BCD′*, Line *NG* would deform to the red parabola. Note ($QS-QW$)$=$$QR$. (B) Shear strain for the *red parabolic profile* on point T_1 is Φ_1.

Using Eqs. (3), (8), and (9):

$$x = 3{*}VtLy(y_0 - Vt)^{-2}\left[1 - y(y_0 - Vt)^{-1}\right] \tag{10}$$

Therefore velocity-wise,

$$V_x = xt^{-1} = 3{*}VLy(y_0 - Vt)^{-2}\left[1 - y(y_0 - Vt)^{-1}\right] \tag{11}$$

Writing V_x henceforth as x, Eq. (3) can be written as, by writing $(y_0 - Vt) = h_t$,

$$(y - 0.5h_t)^2 = -0.33{*}L^{-1}V^{-1}h_t\left(x - 0.75{*}LVh_t^{-1}\right) \tag{12}$$

Coordinate of its vertex is deduced (also recall $h_t = y_0 - Vt$):

$$\left\{0.75LV(y_0 - Vt)^{-1},\ 0.5(y_0 - Vt)\right\} \tag{13}$$

Note (i) the x-ordinate of the vertex of the parabola as in Eq. (11) represents highest speed. (ii) The vertex is equidistant from the two walls at every moment.

The parabolic profile that would be produced by the line MN passing through any point M $(-m, 0)$ lying on the X-axis (Fig. 2A) will be deduced now. If only the rectangle $A'BMN$ were there (Fig. 2A), the distance "M_1" would have been, by replacing "m" in place of "L" in the x-ordinate of Eq. (13),

$$M_1 = 0.75{*}mV(y_0 - Vt)^{-1} \tag{14}$$

If only the rectangle $MNDC$ were there (Fig. 2A), the distance "M_2" would have been, by replacing in place of "L" in the x-ordinate of Eq. (13),

$$M_2 = 0.75{*}(L - m)V(y_0 - Vt)^{-1} \tag{15}$$

The resultant of these two parabolic profiles, in this case both the rectangles $MNDC$ and $A'BMN$ exist side by side and in contact with each other along the line MN:

$$\Delta M = M_1 - M_2 = 0.75{*}(2m - L)V(y_0 - Vt)^{-1},\ \text{if}\ M_1 > M_2 \tag{16}$$

$$\Delta M = M_2 - M_1 = 0.75{*}(L - 2m)V(y_0 - Vt)^{-1},\ \text{if}\ M_1 < M_2 \tag{17}$$

$$\text{And, specifically,}\ \Delta M = 0,\ \text{if}\ m = 0.5{*}L \tag{18}$$

Eq. (18) indicates that, at the middle of the rectangle *ABCD*, the linear inactive marker simply shrinks yet continues as a straight line. Eqs. (16) and (17) indicate that, as one goes at either margins, *AB* and *CD*, one gets parabolic markers with increasing tapering, or in other words, with increasing curvature at their vertices. Second, choosing different values of m ($\leq L$), one can constrain the exact parabolic profile passing through the corresponding point *M*.

C. ***Instruction to the Instructor***: Instruct the student at this point what the meanings of curvature, strain, shear strain, and tangential shear strain are.

Curvature of P_1 is deduced using the standard formula:

$$\rho = \left\{1 + (\mathrm{d}x/\mathrm{d}y)^2\right\}^{3/2} \left(\mathrm{d}^2x/\mathrm{d}y^2\right)^{-1} \tag{19}$$

$$\text{In the present case, } \mathrm{d}x/\mathrm{d}y = 3{*}LV\left(1 - 2{*}yh_t^{\;-1}\right)h_t^{\;-2} \tag{20}$$

$$\text{And } \mathrm{d}^2x/\mathrm{d}y^2 = -6{*}LVh_t^{\;-3} \tag{21}$$

Using Eqs. (20) and (21) in Eq. (19), curvature at the vertex (ρ_v), for which $y = 0.5h_t$ is given by:

$$\rho_v = -0.17h_t^{\;3}L^{-1}V^{-1} \tag{22}$$

This is the highest curvature on the parabola P_1.

Shear strain at any point on the P_1 parabola is studied as follows. As per Fig. 2A, Φ is the angular shear strain at point *T*. Line *TZ* is a tangent on the parabola P_1 drawn at the point *T*.

$$\text{Note } \tan\Phi = \mathrm{Cot}\,\theta = \mathrm{d}x/\mathrm{d}y \tag{23}$$

From Eq. (11),

$$\mathrm{d}x/\mathrm{d}y = 3{*}LVh_t^{\;-2}\left(1 - 2{*}yh_t^{\;-1}\right) \tag{24}$$

$$\text{Therefore } \tan\Phi = 3{*}LVh_t^{\;-2}\left(1 - 2{*}yh_t^{\;-1}\right) \tag{25}$$

Thus Φ and $\tan\Phi$ vary with time inside a pure shear zone. The only exception would be the points on the line that bisects the length of the rectangle (line *GH* in Fig. 2A), where in fact $\Phi = \tan\Phi = 0$ remains time independent. Note, at vertex, that is, for $y = 0.5h_t$ in Eq. (25):

$$\Phi_{\text{vertex}} = 0 \tag{26}$$

This matches with the intuition: at vertex the tangent drawn on the parabola parallels the *Y*-axis, therefore their angle becomes zero.

At origin (0, 0), putting $y = 0$ in Eq. (25),

$$\tan\Phi_{\text{at origin}} = 3{*}LVh_t^{\;-2} \tag{27}$$

And at point A', putting $y = h_t$ in Eq. (25),

$$\tan\Phi_{\text{at } A'} = -3{*}LVh_t^{\;-2} \tag{28}$$

The difference in sign in Eqs. (27) and (28) indicates opposite ductile shear sense. Although at origin it is top-to-right, at A' it is top-to-left. The shear sense flips across the vertex of the parabola.

Strain at any point inside the pure shear zone can also be deduced. With respect to the new coordinate system (Fig. 2B) where the *X*-axis passes through the vertex of the parabola, the equation of the (resultant) parabolic profile can be written as, because it passes through points *N:* $[0, 0.5{*}(y_0 - V{\cdot}t)]$ and M$[0, -0.5{*}(y_0 - V{\cdot}t)]$:

$$x = H\left[y^2 - 0.25{*}(y_0 - V\cdot t)^2\right] \tag{29}$$

At $y = 0$,

$$x = -0.25{*}H(y_0 - V\cdot t)^2 \tag{30}$$

This has to equal ΔM of either Eq. (16) or Eq. (17), therefore,

$$H = -4\Delta M(y_0 - V \cdot t)^{-2} \tag{31}$$

Putting back H in Eq. (29), the parabola is now given by:

$$x = \Delta M\left[1 - 4y^2(y_0 - vt)^{-2}\right] \tag{32}$$

Therefore in the new coordinate system:

$$\tan \Phi_1 = \mathrm{d}x/\mathrm{d}y = -8\Delta M \cdot y(y_0 - vt)^{-2} \tag{33}$$

Putting back the expression of ΔM from Eq. (16) into Eq. (33):

$$\tan \Phi_1 = -6*(2m - L)V(y_0 - Vt)^{-3}y \tag{34}$$

Choose different magnitudes of "m," "y," and "t" to get tangential shear strain $\tan\Phi_1$ (and therefore shear strain Φ_1) at any point inside the pure shear zone. For example, for $y=0$, that is, for the new X-axis bisecting the pure shear zone at any instant (i.e., for any "t"), $\tan\Phi_1 = 0$. This is as expected because, at the vertex of the parabolic profiles, shear strain is zero. Second, for $y = 0.5^*(y_0 - Vt)$, and $m=0$, that is, at point A':

$$\tan \Phi_1 = 3*L \cdot V \cdot (y_0 - Vt)^{-2} \tag{35}$$

2.2 Both the Boundaries Move (Fig. 3A)

Consider the boundaries of shear zones move toward each other at velocities V_1 and V_2 ($V_1 > V_2$). Let AD and AB be, respectively, L and $2y_0$ units long. Points A (0, y_0) and B (0, $-y_0$) on the two walls, after time "t," comes at A' (0, $y_0 - V_1t$) and B' (0, $V_2t - y_0$), respectively. The vertex of the parabola will be equidistant from these two points. Therefore its y-ordinate would be $-0.5^*t(V_1 - V_2)$. Let the x-ordinate of the vertex be p. Thus the complete coordinate is {p, -0.5^*-$t(V_1 - V_2)$}. Let the equation of this parabola be:

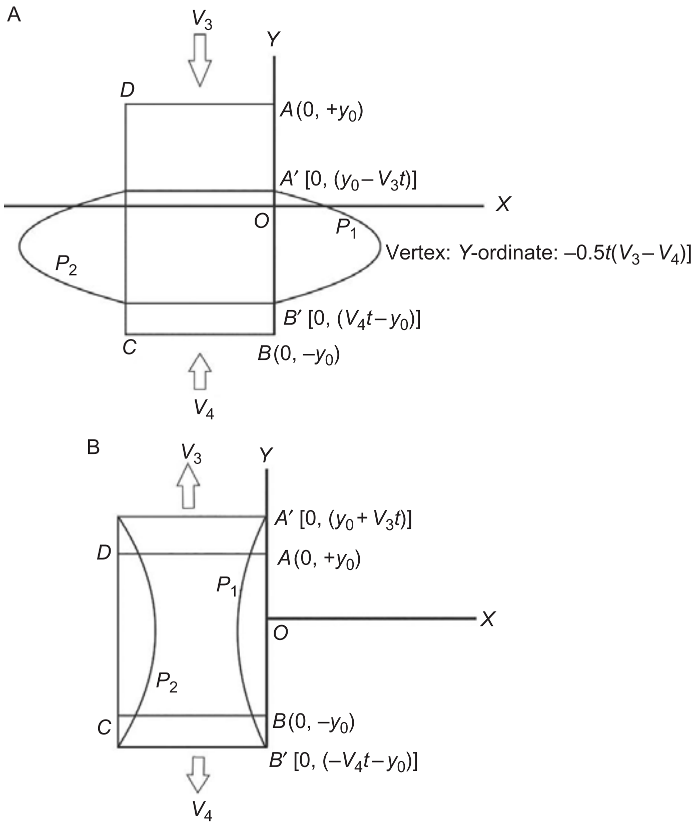

FIG. 3 Pure shear on sides AD with a velocity V_3 and BC with V_4, of the rectangle $ABCD$. After time "t," A reaches A' and B to B'. (A) Compression. (B) Extension.

$$Y^2 + Dx + Ey + F = 0 \tag{36}$$

D. ***Instruction to the Instructor:*** At this point onward, ask the students to proceed themselves. It will be very interesting to see whether they can deduce the velocity profiles!

Putting A' and B' coordinates in Eq. (36), E and F are solved:

$$E = (V_1 - V_2)t \tag{37}$$

$$F = (y_0 - V_1 t)(V_2 t - y_0) \tag{38}$$

Putting them back in Eq. (36):

$$y^2 + D \cdot x + (V_1 - V_2)ty + (y_0 - V_1 t)(V_2 t - y_0) = 0 \tag{39}$$

Area bound by this parabola with the Y-axis between the coordinates {0, $(y_0 - V_1 t)$} and {0, $(V_2 t - y_0)$}:

$$A_1 = \int_{(V_2 t - y_0)}^{(y_0 - V_1 t)} x \, \mathrm{d}x \tag{40}$$

Putting x in Eq. (40) from Eq. (39), and integrating:

$$A_1 = D^{-1}\{2*y_0 - t(V_1 + V_2)\}\left[0.33*\left\{(V_2 - V_1)^2 t^2 + 2(y_0 - V_1 t)(V_2 t - y_0)\right\} - 0.5*t(V_1 + V_2)\right] \tag{41}$$

Area lost due to compression equals area gained at the two sides, being an incompressible fluid under consideration inside the rectangle $ABCD$. Therefore,

$$A_1 = 0.5*(V_1 + V_2)tL \tag{42}$$

Eliminating A_1 from Eqs. (41) and (42):

$$D = 2*t^{-1}L^{-1}(V_1 + V_2)^{-1}\{2*y_0 - t(V_1 + V_2)\}\left[0.33*\left\{(V_2 - V_1)^2 t^2 + 2(y_0 - V_1 t)(V_2 t - y_0)\right\} - 0.5*t(V_1 + V_2)\right] \tag{43}$$

Eliminating D from Eqs. (41) and (43), one gets the resultant parabolic flow profile P_1. In this case also, the vertex will mark the point of minimum shear strain and maximum curvature.

E. ***Instruction to the Instructor:*** By now, one can easily locate students in the classroom who correctly solved and enjoyed taking the challenge. Refer to that small group of students, the two papers, Mukherjee (2012, 2014), and ask them to find out the velocity profile for general shear deformation. This would be a step forward from the title of this article.

3 DISCUSSIONS

Wittenberg (2003) briefly presented shear strain for a sphere pure sheared to an ellipsoid. But unlike the present work, point-to-point variation of shear strain for a pure sheared object, here a rectangle, was not presented by any. Allmendinger et al. (2012) and Zeb et al. (2013) presented kinematic analyses of pure shear zones that especially track fluid particles over time. They did not however provide equations of parabolic velocity profiles produced by such an ideal deformation. Eq. (12) of flow profile for one of the boundary's movement (Case 2A) matches with that presented straightway by Spurk (1999). However, Spurk (1999) did not give the deduction, and to the author's knowledge, it does not exist in any publications. The second deduction of profile for both the boundaries' movement can be obtained by eliminating "D" from Eqs. (41) and (43). This also does not exist in any previous publications. Note the parabolic flow profile also develops for Poiseuille flow of Newtonian viscous fluid through parallel-sided boundaries. However, in that case, the profile becomes time-independent (Mukherjee, 2012). This is unlike pure shear where the curvature at every moment at the vertex is a (cubic) function of time (such as Eq. 22). Changing shear strain with time inside shear zones is also known in real cases (e.g., Grasemann et al., 1999). Note that, by putting $V_2 = 0$ in Eqs. (41) and (43) and then eliminating "D," one would *not* simply go back to Eq. (12): the case of movement of a single boundary. This is because, in the two cases, the origins (0, 0) were selected differently.

In one case, the sides of the rectangular pure sheared rectangle is completely rigid and precludes flow materials outward due to the presence of some massive geological body; Eqs. (7) and (42) alter respectively to:

$$A_1 = LVt \tag{44}$$

$$A_1 = (V_1 + V_2)tL \tag{45}$$

Accordingly the flow profiles (Eqs. 12, 41, and 43 after elimination of "D"), shear strain pattern (Eq. 25) inside the pure shear zone, and the curvature of the profile (Eq. 22) would change.

In case both the boundaries move with equal velocity U ($=V_1=V_2$), Eqs. (41) and (43) simplify, respectively to:

$$y^2 + D \cdot x - (y_0 - Ut)^2 = 0 \tag{46}$$

$$D = -4L^{-1}(y_0 - tU)^3 \tag{47}$$

Eliminating "D" from Eqs. (46) and (47), the parabolic profile becomes:

$$y^2 - 4L^{-1}(y_0 - tU)^3 \cdot x - (y_0 - tU)^2 = 0 \tag{48}$$

The Y-ordinate of its vertex is "y_0." This means that the vertex is not only equidistant temporally from both the moving walls but maintains its initial position. This is unlike the situations when *(i)* one of the walls is static (*Case 2A*) and *(ii)* both the walls move with unequal velocities ($V_1 \neq V_2$ situation in *Case 2B*). Note Eq. (48) cannot be compared straightway with Eq. (12) by merely considering $2U = V$, because the coordinate systems of *Cases 2A* and *2B* differ. In case the boundaries move away from each other in a pure shear manner, the coordinates of the points A', B' etc. should be obtained first (Fig. 3B) and then proceed in the same way to deduce flow profiles. In this case, the convex sides of the two parabolic margins are toward the center of the rectangle.

The deductions presented here work obviously under several presumptions. Because rocks have quite low compressibility (2.55*10^{-11} Pa^{-1} for sediments: Turgut, 1997), considering it to be incompressible looks justified. However, in a bit different context, layer perpendicular compression of sediments in basins due to their own weights ("gravitational compaction": Wangen, 2010) can reduce volume (Mukherjee and Kumar, in press). Shear zone boundaries would be rigid if the ratio of viscosity between the shear zone and its surroundings is $\leq 10^{-7}$. Melting and other fluid activities during ductile shearing can significantly reduce volume of the shear zones. Ultra-high-pressure rocks under dissolution-precipitation creep and granular flow at low stress act as Newtonian fluids (review in Mukherjee, 2012; Mukherjee and Mulchrone, 2012). Likewise, natural granitic melt can be a Newtonian fluid, but this is not necessarily true for all kinds of crustal melts. Natural shear zones can obviously contain more than one lithology. Viscous dissipation might elevate temperature that might modify the parabolic profile. Unlike constant V considered in *Case 2A* and constant V_1 and V_2 in *Case 2B*, the movement rate of boundaries of shear zones can vary in nature (e.g., Janecke et al., 2010).

This work deduces kinematics of a horizontal pure shear zone (Figs. 2A and 3A). Horizontal (Mies, 1991) and sub-horizontal ductile shear zones (Lister and Davis, 1989) have been referred by many from nature. In reality, shear zones can dip (Jégouzo, 1980), and in that case, the effect of gravity needs to be considered in the kinematic analysis.

Elliptical symmetric quartz blebs, symmetric pressure shadows and fringes indicate pure shear, although asymmetric fabrics can also be produced by simple shear (Mukherjee, 2017 and references therein). Myrmekitization-induced augen in ductile shear zones indicate volume loss (e.g., Menegon et al., 2008), therefore the presented model for constant area (and volume) deformation would not work there. Also, augens can indicate heterogeneous deformation (Dell'Angello and Tullis, 1989) that would restrict the use of the presented model.

Acknowledgments

A research sabbatical for the year 2017 and a CPDA grant provided by IIT Bombay are thanked. This work bases preliminary analysis of pure shear in Mukherjee (2007). Thanks to Amy Shapiro, Tasha Frank, and the proofreading team (Elsevier), and Ake Fagereng (University of Cardiff) and Andrea Billi (Sapienza Universita di Roma) for reviewing and handling this chapter. I dedicate this article to Late Profs. Gaurishankar Ghatak and Malay Bhushan Chakrabarti for their exhaustive teaching of fundamentals of geology during SM's B.Sc. program in the then-Presidency College, Kolkata during 1996–99.

References

Allmendinger, R.W., Cardozo, N., Fisher, D.M., 2012. Structural Geology Algorithms: Vectors and Tensors. Cambridge Univ. Press, Cambridge, pp. 183–199.

Bailey, C.M., Polvi, L.E., Forte, A.M., 2007. Pure shear dominated high-strain zones in basement terrains. In: Hatcher Jr., R.D., Carlson, M.P., McBride, J.H. (Eds.), 4-D Framework of Continental Crust. Geol. Soc. Am. Mem., vol. 200, pp. 93–108.

Bose, N., Dutta, D., Mukherjee, S., 2018. Role of grain-size in phyllonitisation: insights from mineralogy, microstructures, strain analyses and numerical modeling. J. Struct. Geol. 112, 39–52.
Dell'Angello, L.N., Tullis, J., 1989. Fabric development in experimentally sheared quartzites. Tectonophysics 169, 1–21.
Dennis, J.G., 1987. Structural Geology: An Introduction. William C Brown Publication, p. 134, ISBN-10: 0697001334.
Fossen, H., 2016. Structural Geology, second ed. Cambridge University Press, Amsterdam, ISBN: 978-1-107-05764-7, pp. 49–50.
Fossen, H., Cavalcante, G.C.G., 2017. Shear zones—a review. Earth-Sci. Rev. 171, 434–455.
Gere, J.M., Goodno, B.J., 2012. Mechanics of Materials, eighth ed. Cengage Learning, Stamford, p. 193.
Grasemann, B., Fritz, H., Vannay, J.-C., 1999. Quantitative kinematic flow analysis from the Main Central Thrust Zone (NW-Himalaya, India): implications for a decelerating strain path and the extrusion of orogenic wedges. J. Struct. Geol. 21, 837–853.
Hobbs, B.E., Ord, A., 2014. Structural Geology: The Mechanics of Deforming Metamorphic Rocks. Elsevier, Amsterdam.
Howarth, R.J., 2017. Dictionary of Mathematical Geosciences: With Historical Notes. Springer, Cham, p. 557.
Jaeger, J.C., 1969. Elasticity, Fracture and Flow. John Wiley & Sons, New York, NY.
Janecke, S.U., et al., 2010. High geologic slip rates since Early Pleistocene initiation of the San Jacinto and San Felipe Fault Zones in the San Andreas Fault System: Southern California, USA. Geol. Soc. Am. Spec. Pap. 475. 48 p.
Jégouzo, P., 1980. The south Armorican shear zone. J. Struct. Geol. 2, 39–47.
Lister, G.S., Davis, G.A., 1989. The origin of metamorphic core complexes and detachment fault formed during Tertiary continental extension in the northern Colorado river region, U.S.A. J. Struct. Geol. 11, 65–94.
Lopez-Mir, B., 2018. Cross-section construction and restoration: examples from the Pyrenees and the Canadian Arctic. In: Billi, A., Fagereng, A. (Eds.), Problems and Solutions in Structural Geology and Tectonics. Developmentsin Structural Geology and Tectonics Book Series. Series Editor: Mukherjee S.. Elsevier. ISSN: 2542-9000.
Malkin, A.Y., Isayev, A.I., 2006. Rheology: Concepts, Method and Applications., third ed. Chem Tech Publishing, Toronto, pp. 31–33.
Manga, M., 2005. Deformation of flow band by bubbles and crystals. In: Manga, M., Ventura, G. (Eds.), Kinematics and Dynamics of Lava Flows. Geol. Soc. Am. Spec. Pap., vol. 396, pp. 47–53.
Menegon, K., Pennacchioni, G., Spiess, R., 2008. Dissolution-precipitation creep of K-feldspar in mid-crustal granite mylonites. J. Struct. Geol. 30, 565–579.
Mies, J.W., 1991. Planar dispersion of folds in ductile shear zones and kinematic interpretation of fold-hinge girdles. J. Struct. Geol. 13, 281–297.
Mukherjee, S., 2007. Geodynamics, Deformation and Mathematical Analysis of Metamorphic Belts, NW Himalaya (Ph.D. thesis). Indian Institute of Technology, Roorkee, pp. 75–149.
Mukherjee, S., 2012. Simple shear is not so simple! Kinematics and shear senses in Newtonian viscous simple shear zones. Geol. Mag. 149, 819–826.
Mukherjee, S., 2013. Channel flow extrusion model to constrain dynamic viscosity and Prandtl number of the Higher Himalayan Shear Zone. Int. J. Earth Sci. 102, 1811–1835.
Mukherjee, S., 2014. Kinematics of 'top -to-down' simple shear in a Newtonian rheology. J. Indian Geophys. Union 18, 245–248.
Mukherjee, S., 2017. Review on symmetric structures in ductile shear zones. Int. J. Earth Sci. 106, 1453–1468.
Mukherjee, S., Kumar, N., in press. A first-order model for temperature rise for uniform and differential compression of sediments in basins. Int. J. Earth Sci. https://doi.org/10.1007/s00531-018-1634-6.
Mukherjee, S., Mulchrone, K., 2012. Estimating the viscosity and Prandtl number of the Tso Morari Gneiss Dome, western Indian Himalaya. Int. J. Earth Sci. 101, 1929–1947.
Mulchrone, K.F., Mukherjee, S., 2016. Kinematics and shear heat pattern of ductile simple shear zones with 'slip boundary condition'. Int. J. Earth Sci. 105, 1015–1020.
Papanastasiou, T.C., Georgiou, G.C., Alexandrou, A.N., 2000. Viscous Fluid Flow. CRC Press, Boca Raton, FL, pp. 387–389.
Passchier, C.W., Trouw, R.A.J., 2005. Microtectonics, second ed. Springer. ISBN 978-3-540-29359-0.
Ramsay, J.G., Lisle, R., 2000. The Techniques of Modern Structural Geology. Applications of Continuum Mechanics in Structural Geology, Vol. 3. Academic Press, San Francisco, CA, p. 926.
Regenauer-Lieb, K., Yuen, D.A., 2003. Modeling shear zones in geological and planetary sciences: solid-and fluid-thermal-mechanical approaches. Earth-Sci. Rev. 63, 295–349.
Reitan, P.H., 1987. Strain. In: Seyfert, C.K. (Ed.), The Encyclopedia of Structural Geology and Plate Tectonics. Van Nostrand Reinhold Company, New York, NY, pp. 738–746.
Schlichting, H., 1960. Boundary Layer Theory, fourth ed. McGraw-Hill, New York.
Segal, V.M., 2002. Severe plastic deformation: simple shear vs. pure shear. Mater. Sci. Eng. A 338, 331–344.
Spurk, J.H., 1999. Fluid Mechanics: Problems and Solutions. Springer-Verlag, Berlin, pp. 56–58.
Treagus, S.H., Lan, L., 2000. Pure shear deformation of square objects, and applications to geological strain analysis. J. Struct. Geol. 22, 105–122.
Turgut, A., 1997. Inversion of bottom/subbottom statistical parameters from acoustic backscatter data. J. Acoust. Soc. Am. 102, 833–852.
Twiss, R.J., Moores, E.M., 2007. Structural Geology. W. H. Freeman & Company, New York, NY, p. 340.
Wangen, M., 2010. Physical Principles of Sedimentary Basin Analysis. Cambridge Univ. Press, Cambridge, pp. 90–91.
Wittenberg, R., 2003. On geodetic description of 3D-body-deformation. In: Grafarend, E.W., Krumm, F.W., Scwarze, V.S. (Eds.), Geodesy: The Challenges of the Third Millennium. Springer, New York, pp. 401–404.
Xypolias, P., 2010. Vorticity analysis in shear zones: a review of methods and applications. J. Struct. Geol. 32, 2072–2092.
Zeb, A., Siddiqui, A.M., Ahmed, M., 2013. An analysis of the flow of a Newtonian fluid between two moving parallel plates. ISRN Math. Anal. 2013, Article ID 535061.